# Activating Surface Lattice Oxygen of a $Cu/Zn_{1-x}Cu_xO$ Catalyst through Interface Interactions for CO Oxidation

*Minli Zeng*[†], *Xiyang Wang**[,‡], *Qilei Yang*[c], *Xuefeng Chu**[,§], *Zuolong Chen*[‡], *Zhen Li*[†], *Carl Redshaw*[⊥], *Chao Wang*[//], *Yue Peng*[§], *Nannan Wang**[,†], *Yanqiu Zhu*[†], *and Yimin A.Wu*[‡]

† Guangxi Institute Fullerene Technology (GIFT), Key Laboratory of New Processing Technology for Nonferrous Metals and Materials, Ministry of Education, School of Resources, Environment and Materials, Guangxi University, Nanning, 530004, P. R. China

‡ Department of Mechanical and Mechatronics Engineering, Waterloo Institute for Nanotechnology, Materials Interface Foundry, University of Waterloo, Waterloo, Ontario N2L 3G1, Canada

§ School of Environment, Tsinghua University, Beijing 100084, P. R. China

// Key Laboratory of Architectural Cold Climate Energy Management, Ministry of Education, Jilin Jianzhu University, Changchun 130118, P. R. China

⊥ Plastics Collaboratory, Department of Chemistry, University of Hull, Hull HU6 7RX, UK

*Email: xiyang.wang@uwaterloo.ca.

*Email: stone2009@126.com.

*Email: wangnannan@gxu.edu.cn.

Keywords

surface lattice oxygen, interface interactions, Active sites, CO oxidation, reaction mechanism

Abstract

Surface lattice oxygen in metal oxides is a common participant in many chemical reactions. Given this, the structural design of catalysts to activate lattice oxygen and moreover investigations into the effect of lattice oxygen on reaction pathways are hot topics. With this in mind, herein we prepare CuO-$Zn_{1-x}Cu_xO$ (ZCO) nanofibers akin to the Trojan horse legend and via an in situ reduction obtain activated Cu/$Zn_{1-x}Cu_xO$ (Cu/ZCO) nanofibers. X-ray absorption spectroscopy and X-ray photoelectron spectroscopy reveal that surface lattice oxygen of Cu/ZCO is effectively activated from inert $O^{2-}$ to reactive $O^{2-x}$. This activation stems from the enhanced covalence of metal-oxygen bond and the electron transfer between Cu and the support. Online mass spectrometry reveals that Cu/ZCO with activated lattice oxygen exhibits a higher Mars-van Krevelen reaction efficiency during the CO oxidation process. This study offers a new avenue to engineer interface interactions, given, as highlighted here, the importance of surface lattice oxygen in oxide supports during the catalytic process.

TOC

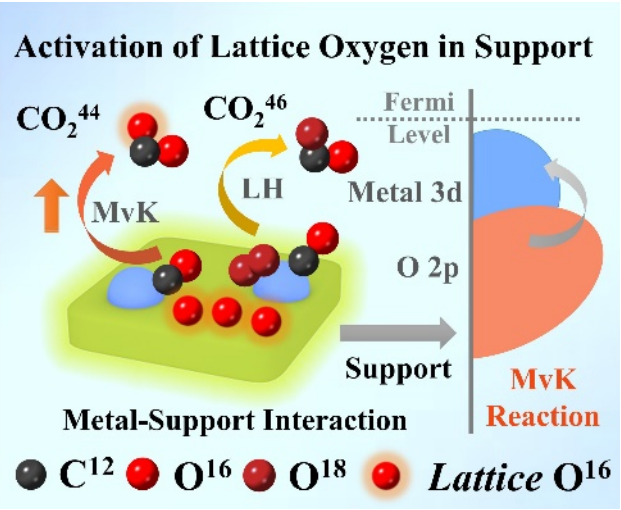


Herein, we have developed a strategy similar to the Trojan horse to engineer Cu/Zn1-*x*Cu*x*O materials with metal-support interactions, where the covalency of the metal-oxygen bond in the support is enhanced and there is also strong electron transfer between the Cu nanoparticles and the support. The optimization of the electronic structure efficiently activates the surface lattice oxygen of the support and improves the catalytic activity and durability. Online isotopic mass spectrometry clarifies that the activated surface lattice oxygen dramatically increases the catalytic efficiency of the MvK mechanism but has no obvious effect on the L–H mechanism during the CO oxidation process.

Introduction

The reactivity of surface lattice oxygen in transition metal oxides has a significant influence on the performance of a catalytic reaction process.[1-3] For example, reversible, active, and stable anion redox properties of a lattice oxygen can increase the capacity of a lithium ion battery, improve the catalytic efficiency of the Mars-van Krevelen (MvK) mechanism in thermocatalysis or the lattice oxygen oxidation mechanism in the oxygen evolution reaction.[4-7] In general, surface lattice oxygens of intrinsic transition metal oxides are relatively inert. To improve the catalytic performance and durability, the surface lattice oxygen of a solid catalyst needs efficient activation using a suitable method.[5, 8, 9] In recent years, the engineering of surfaces/interfaces and manipulation of the electronic structure of transition metal oxides have received increased attention to improve the activity of the surface lattice oxygen. Despite such studies, the activation of surface lattice oxygen remains a challenge for many catalytic reactions.

The chemical properties of surface lattice oxygen tend to be dominated by the covalence of the metal-oxygen interactions.[6, 10, 11] Common strategies for regulating the covalence involve cationic or oxygen architectural defects, element doping, crystal facet design, surface modification, and tuning of the charge transfer in the composite materials.[3, 5, 11-15] One of the most popular activating methods involves dispersing metal nanoparticles or single atoms at the surface of metal oxides, where the interaction between the two phases can optimize the hybridization of the metal-oxygen bond via electron transfer between the metal and support.[16-18] An example is the use of a single Pt atom at the twisted surface of $CeO_2$, M/$TiO_2$ (M=Pt, Fe, Mn, Co, Ni, Cu), Cu/$CeO_2$, M/ZnO (M = Au, Pt, Cu), and so on.[3, 8, 19-22] Currently, the preferred method for the preparation of metal/support catalysts utilizes impregnation and atomic layer deposition.[16, 19, 23] Different from traditional preparation methods, exsolution processes provide new opportunities to tailor stable metal-oxide interfaces and to improve activity and stability.[24] Exsolved metal particles based on Ni, Co, Fe, Pd, and Pt have successfully been synthesized via this pathway, and the resulting tailored catalysts

exhibited better catalytic performances.[25-27] A similar exsolution route may address this issue in other metal/support catalysts.

Promising catalysts based on Cu/ZnO materials have gained increasing prominence because of their impressive catalytic performances during $CO_2$ hydrogenation, CO oxidation, and the water–gas shift reaction.[21, 28-30] However, the impact of the interface effect between Cu and the ZnO support on the various catalytic processes remains elusive, particularly the role played by the surface lattice oxygen.[21, 28, 29] Recently, it has been reported, via the use of online isotopic mass spectrometry, that the activity of the surface lattice oxygen in other transition metal oxides plays an important role in dictating the reaction pathway and influencing the active sites.[31-33] With this in mind, we herein employ online isotopic mass spectrometry to monitor reaction products and to analyze the mechanism associated with the CO oxidation process. Moreover, we hoped to identify the true active sites in the constructed Cu/ZnO materials.

We present herein an electrostatic spinning method for the preparation of mixed CuO-$Zn_{1-x}Cu_xO$ (ZCO) nanofibers, where the CuO in the Trojan horse (ZCO) is in situ reduced to Cu metal nanoparticles thereby forming Cu/$Zn_{1-x}Cu_xO$ (Cu/ZCO) composite catalysts by hydrogen annealing at high temperature. The regulated Cu/ZCO catalyst reveals clear interface interactions between the Cu and ZCO. Indeed, surface sensitive tools (X-ray absorption spectroscopy (XAS) and X-ray photoelectron spectroscopy (XPS)) demonstrate that there is electron transfer between the two phases, which is able to tune the covalence of the Zn/Cu-O bond and improve the activity of the surface lattice oxygen. By contrast, a mechanically mixed Cu-ZCO sample only displayed the average effect for the electronic structure, while surface lattice oxygen is not activated. The use of online isotopic mass spectrometry illustrates that the active surface lattice oxygen in the support can improve reaction efficiency for the MvK mechanism. Therefore, it is evident that the

Cu/ZCO catalyst possesses better catalytic activity and durability for CO oxidation. The present study reveals that the surface lattice oxygen in inert oxide supports also becomes an important active site beyond the traditional metal cation site.

## Results and discussion

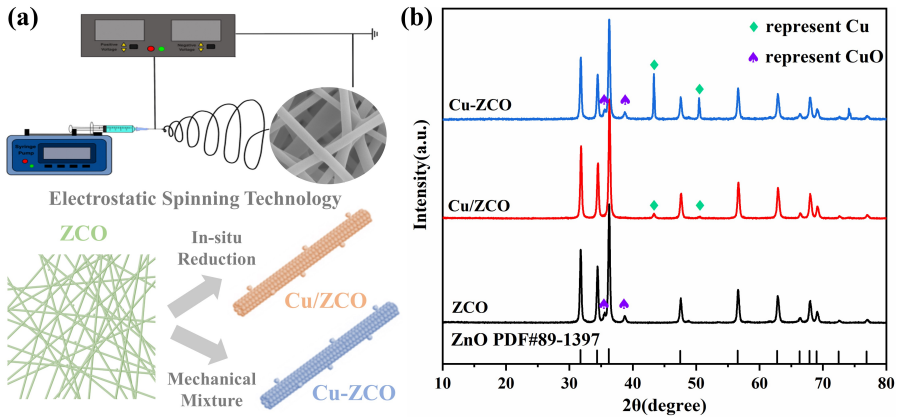


**Figure 1.** (a) Schematic illustration of the synthetic routes for ZCO, Cu/ZCO, and Cu-ZCO; (b) X-ray diffraction (XRD) patterns for ZCO, Cu/ZCO, and Cu-ZCO in which green represents the Cu metal nanoparticles and purple represents the CuO structure.

As shown in **Figure 1 a**, the ZCO sample was synthesized by the electrospinning method. The synthetic process is displayed in the Experimental Section in the Supporting Information. After $H_2$ annealing, the entrained CuO in the Trojan horse (ZCO) was reduced *in-situ* into Cu metal nanoparticles to form the Cu/ZCO composite catalyst.[34] The reference sample Cu-ZCO was prepared by mechanically mixing some Cu nanoparticles in ZCO. The powder XRD patterns of the as-prepared ZCO, Cu/ZCO, and Cu-ZCO catalysts are shown in **Figure 1 b**. All the diffraction peaks are indexed with reference to the hexagonal ZnO structure (Hexagonal, *P63mc*) in which the peaks at $2\theta = 35.5°$ and 38.8° in the ZCO and Cu-ZCO spectra represent the characteristic

diffraction peaks of the CuO material (monoclinic, C2/c). The diffraction peaks at 43.3° and 50.5° for Cu/ZCO and Cu-ZCO respectively represent the characteristic diffraction peaks of Cu metal nanoparticles. Compared with the ZCO nanofiber, the CuO diffraction peak in Cu/ZCO disappears and the Cu peak increases in the XRD patterns. These results demonstrate the target phase structure and the loading of the Cu metal nanoparticles, which is consistent with our design goal in **Figure 1 a**. Furthermore, element content of these samples is measured using inductively coupled plasma (ICP) and scanning electron microscopy energy-dispersive X-ray spectroscopy (SEM-EDS). These analysis results are displayed in **Figures S1-S3** and **Table S1**, respectively. According to the ICP calculation method, the ratio of Zn/Cu composite in ZCO, Cu-ZCO, and Cu/ZCO is 11.3, 7.1, and 9.7, respectively. The SEM-EDS result shows that the ratio of the Zn/Cu is 8.9 (ZCO), 6.6 (Cu-ZCO), and 15.6 (Cu/ZCO), respectively. Generally, ICP is responsible for analyzing the element composite in the integral solid material, while SEM-EDS data depend on the local composite information and have suitable limitation of space resolution. Therefore, these test results show some difference in the element ratio because of the test principle and systematic and experimental errors.

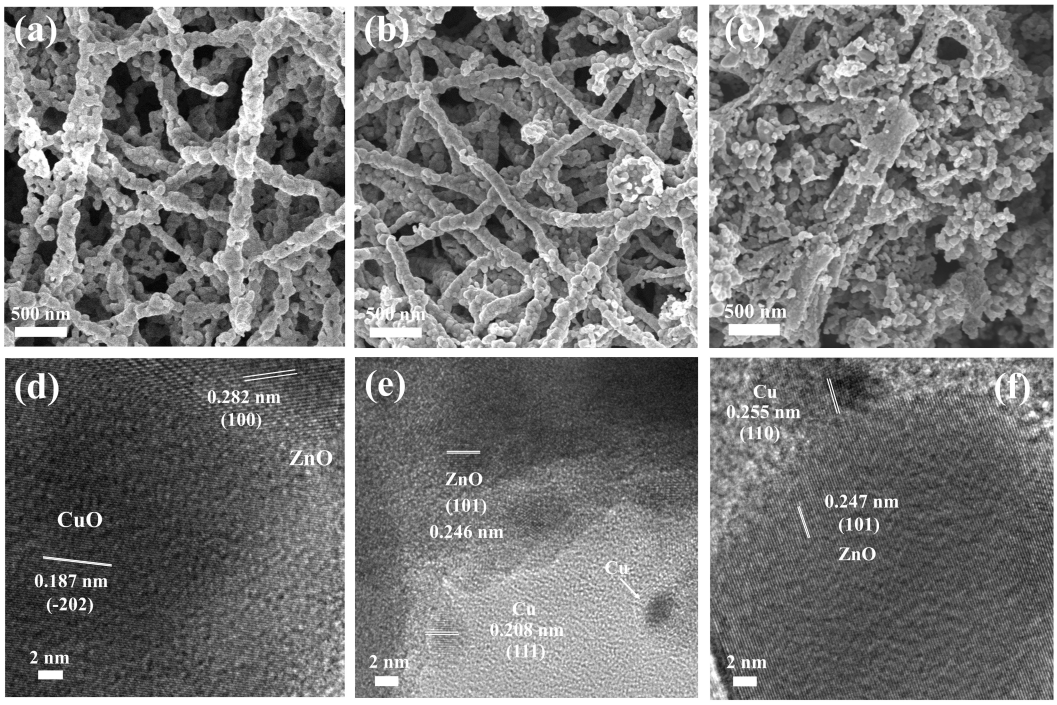


**Figure 2.** SEM images of (a) ZCO nanofibers, (b) Cu/ZCO nanofibers, and (c) mechanically mixed Cu-ZnO; high-resolution transmission electron microscopy (HRTEM) images of (d) ZCO nanofibers, (e) Cu/ZCO nanofibers, and (f) mechanically mixed Cu-ZnO.

The surface morphology of these samples was characterized using scanning electron microscopy (SEM). As shown in **Figure 2 a-c**, ZCO, Cu-ZCO, and Cu/ZCO are one-dimensional long nanofibers and these catalysts are similar to each other in terms of morphology and size. The nanofiber is composed of many nanoparticles and the fiber diameter is about 170 nm. The average size of the nanoparticle in the nanofibers is about 70 nm. **Figure 2 b** demonstrates that *in-situ* annealing fails to change the original fiber morphology. In **Figure 2 c**, it is also evident that the mechanically mixed Cu-ZCO possesses other nanoparticles at the surface. Furthermore, the morphology of these materials was also measured using TEM. As displayed in **Figure S4**, the TEM images for ZCO, Cu-ZCO, and Cu/ZCO reveal similar morphology and size for the integral nanoparticles. In addition, HRTEM images were obtained to further elucidate the crystal structure of these samples, which were confirmed by measuring the lattice spacing in the HRTEM images.

**Figure 2 d-f** show that the ZCO is composed of CuO and ZnO, while Cu/ZCO and Cu-ZCO consist of Cu nanoparticles and ZCO. These results are in accordance with the XRD results.

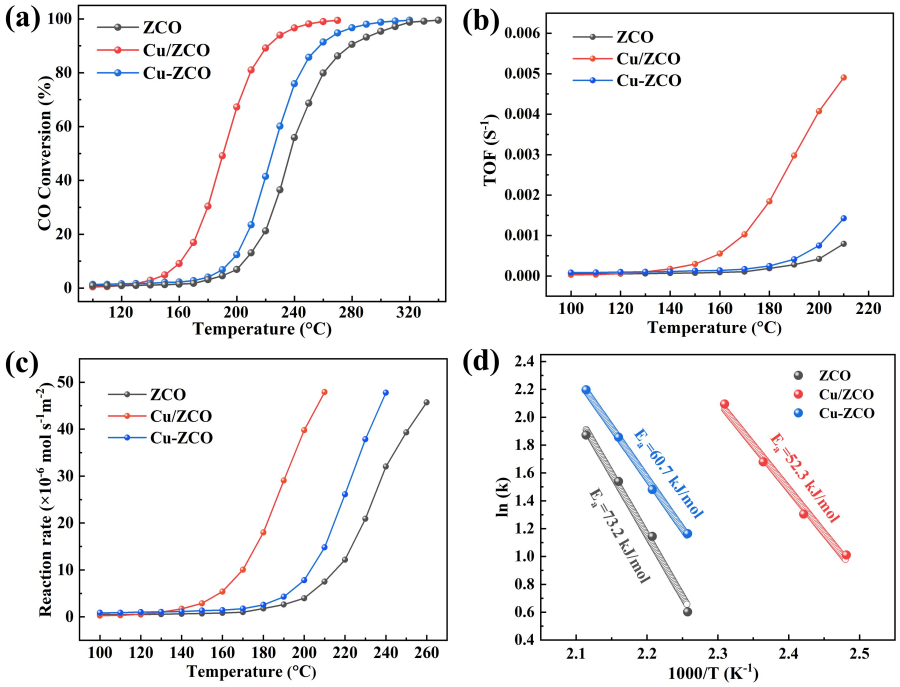


**Figure 3.** (a) CO oxidation activity, (b) temperature-dependent turnover frequencies (TOFs) for CO oxidation normalized by the number of Cu active sites, (c) reaction rate normalized by the specific surface area of the catalysts, and (d) Arrhenius plots of the rate constants for ZCO, Cu/ZCO, and Cu-ZCO.

To assess the catalytic activity of these samples, CO oxidation conversion curves at different temperatures were recorded. **Figure 3a** shows that Cu/ZCO possesses a lower light-off temperature than both ZCO and Cu-ZCO, indicating better CO oxidation activity. In particular, **Figure S5** shows that Cu/ZCO has lower CO conversion temperatures of $T_{10}$, $T_{50}$, and $T_{90}$, which are 161, 190, and 222 °C, respectively. Mechanically mixed Cu-ZCO also exhibited a decrease in $T_{10}$ (196 °C), $T_{50}$ (224 °C), and $T_{90}$ (257 °C) when comparing with ZCO (206, 237, and 278 °C). To avoid the effect of the calcination process on catalytic performance, Cu-ZCO-B is calcined first

and then mechanically mixed. **Figure S6** shows that the catalytic performance errors of pre-annealing and post annealing are acceptable ~6 °C. To investigate the intrinsic activity of the catalysts, TOFs for ZCO, Cu/ZCO, and Cu-ZCO were calculated using the relevant equation – see the experimental section. **Figure 3 b** shows that Cu/ZCO possesses higher values for TOFs for the CO oxidation than both ZCO and Cu-ZCO at different reaction temperatures. The mechanically mixed Cu-ZCO exhibited only a small increase in TOF values. This result is consistent with the CO oxidation data and confirms that the reactive site in Cu/ZCO possesses higher reactivity. Furthermore, the CO oxidation reaction rates normalized by the specific surface area were also calculated to study the intrinsic catalytic activity of these materials and eliminate the effect of the specific surface area on catalytic performance. Therefore, the specific surface area of ZCO, Cu/ZCO, and Cu-ZCO was measured using nitrogen adsorption apparatus; results are 12.9, 12.6, and 11.8 $m^2g^{-1}$, respectively (**Figures S7 and S8**). The calculated results for the reaction rates are shown in **Figure 3 c**. It was observed that Cu/ZCO has a higher reaction rate (mol $s^{-1}$ $m^{-2}$) at different temperatures compared to Cu-ZCO and ZCO, indicating a higher intrinsic catalytic activity for Cu/ZCO. In addition, the activation energy calculated by Arrhenius plots of the rate constants was used to analyze the intrinsic catalytic activity. **Figure 3 d** shows that Cu/ZCO possesses a lower activation energy for CO oxidation (~52.3 kJ $mol^{-1}$) versus ZCO and Cu-ZCO, which is 60.7 and 73.2 kJ $mol^{-1}$, respectively. These results unanimously demonstrate that the reactive sites in Cu/ZCO have higher activity, which dramatically improves the intrinsic catalytic activity for CO oxidation. To investigate the durability of the reactive sites in these catalysts, the CO oxidation process was performed uninterruptedly over 36 h at a reaction temperature of 230 °C. **Figure S9** shows the test results for ZCO, Cu/ZCO, and Cu-ZCO durability at a flow rate of 100 mL/min. It was observed that the CO oxidation activity of ZCO markedly decreased on prolonging the reaction time, while Cu-ZCO and Cu/ZCO exhibited excellent stability. After 36 h

of measurements, the catalytic performance of ZCO had declined by ~10.2%, while for Cu/ZCO and Cu-ZCO the decrease was ~1.4 and ~4.1% during the CO oxidation process. These catalytic data demonstrates that the surface sites in Cu/ZCO are more active and flexible during the dynamic reaction of CO oxidation *versus* those in ZCO and Cu-ZCO.

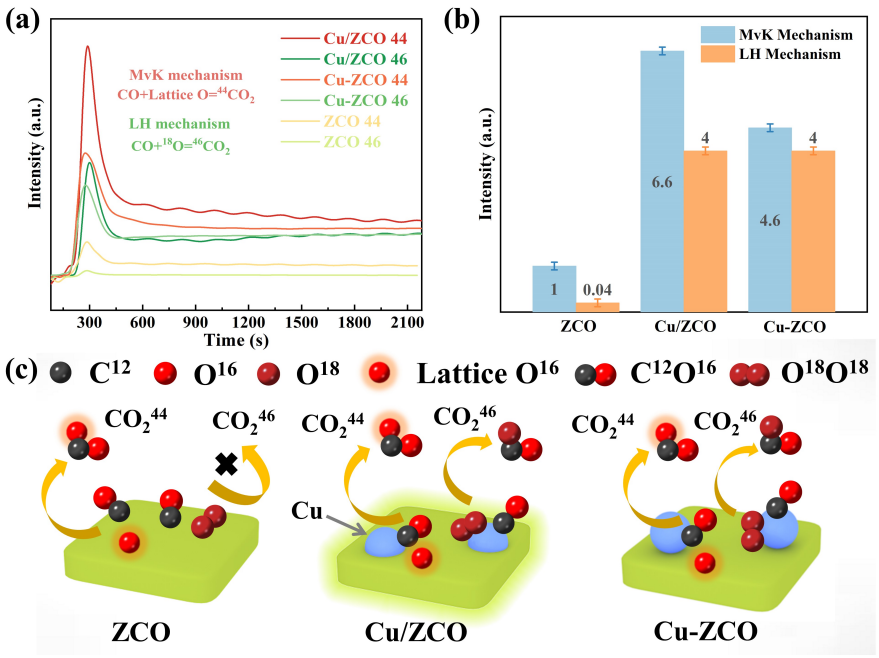


**Figure 4.** (a) On-line mass spectrometry signals for ZCO, Cu/ZCO, and Cu-ZCO in CO oxidation at 220 °C, where $O_2^{36}$, $CO^{28}$, and lattice $O^{16}$ in the catalysts as reactant reagents are conversed into $CO_2^{44}$, $CO_2^{46}$, and $CO_2^{48}$ during the catalytic process. (b) Normalized reaction efficiency of MvK and the L-H mechanism for ZCO, Cu/ZCO, and Cu-ZCO. (c) Schematic illustration of two reaction pathways for MvK and the Langmuir-Hinshelwood (L-H) mechanism in ZCO, Cu/ZCO, and Cu-ZCO for CO oxidation, where $O^{16}$ and $O^{18}$ are lattice oxygen and oxygen, respectively.

To deeply study the reaction mechanism of the catalysts during CO oxidation, online mass spectrometry was employed to identify routes to the production of $CO_2$,$^{44}$ $CO_2$,$^{46}$ and $CO_2$,$^{48}$ where $O_2^{36}$, CO,$^{28}$ and lattice $O^{16}$ in the catalysts are considered as reactant gas. As shown in **Figure 4 a**, signals for $CO^{30}$ and $CO_2^{48}$ were not detected during the CO oxidation process, which suggests

that the CO molecule is not easily dissociated into C* and O* at the surface of these catalysts. For all the materials, the $CO_2^{44}$ signal was readily detected by online mass spectrometry, which is consistent with the participation of the lattice oxygen ($O^{16}$) of the catalysts in the oxidation reaction, and further indicates that this catalytic reaction proceeds by a MvK mechanism.[7] Moreover, the intensity of the $CO_2^{44}$ signal in the mass spectrometry increases remarkably on going from ZCO to Cu-ZCO to Cu/ZCO. This result clarifies that interface interactions can activate surface lattice oxygen to improve the efficiency of the MvK catalytic mechanism and the in situ reduced Cu/ZCO akin to the Trojan horse legend; that is, this system exhibits a higher efficiency for the MvK mechanism than does mechanically mixed Cu-ZCO. The differing results for the $CO_2^{46}$ signal in the mass spectrometry *versus* $CO_2^{44}$ and $CO_2^{48}$ can be attributed to the oxidation reaction of CO and $O_2^{36}$ in the L-H mechanism.[31] It can be seen that Cu-ZCO and Cu/ZCO have similar intensity for the $CO_2^{46}$ signal, which are much higher than that in the ZCO sample. This indicates that the key effect of the Cu nanoparticle is to facilitate the dissociation of CO and $O_2$, which improves the catalytic efficiency of the L-H mechanism. During the CO catalytic oxidation process, lattice $O^{16}$ in the catalyst would be consumed gradually and some $O^{18}$ was filled into the oxygen vacancy in the catalyst. After the next catalytic reaction, the refilled $O^{18}$ will be consumed again. Therefore, the curves of $CO_2^{46}$ signal of Cu/ZCO in MS measurement have a slow rise and the intensity of the $CO_2^{44}$ curve has a decrease. To better understand the relationship between the structure and the reaction mechanism, the normalized reaction efficiency and a schematic illustration of the two reaction pathways for MvK and the L-H mechanism are presented. As shown in **Figures 4 b** and **4 c**, the CO catalytic oxidation process of ZCO is dominated by the MvK mechanism and it is difficult for the $O_2$ to dissociate. The introduction of the Cu nanoparticles can improve the efficiency of these two mechanisms because CO is adsorbed on the surface of Cu. Therefore, we propose that Cu nanoparticles can decrease the activation energy of CO dissociation

in these two mechanisms and also improve the ability for $O_2$ dissociation in the L-H mechanism. On comparing Cu-ZCO with Cu/ZCO, it is very clear that the latter has higher efficiency in the MvK mechanism, while similar ability for the L-H mechanism (**Figure 4 b**). These important data reveal that the surface lattice oxygen in Cu/ZCO is efficiently activated by enhancing the electron transfer between the metal and the support, and this is helpful in decreasing the energy barrier of the lattice oxygen reaction in the MvK mechanism of the CO oxidation. Furthermore, in situ diffuse reflectance infrared Fourier transform spectroscopy (DRIFTS) spectra of CO adsorption over ZCO, Cu-ZCO, and Cu/ZCO at different times are characterized, respectively. As shown in **Figures S10-S12**, the peak located at ~2360 $cm^{-1}$ can be ascribed to the formation of $CO_2$, and the peaks observed in the range of 1300-1650 $cm^{-1}$ are carbonate and formate species.[35, 36] In contrast, the band at ~2110 $cm^{-1}$ and at ~2170 $cm^{-1}$ can be considered as CO adsorption on the Cu site and Zn site, respectively.[37] It's found that ZCO has more adsorbed carbonate species than Cu-ZCO and Cu/ZCO, which indicates that the Cu/ZCO surface has a weaker adsorption for $CO_2$ or carbonate species. We also observe that adsorbed CO in the Cu site of Cu/ZCO has a shift to high wavenumber compared with Cu-ZCO and ZCO. This important result may stem from the enhancement of Cu-O bonds or the charge transfer between the metal and ZCO support.

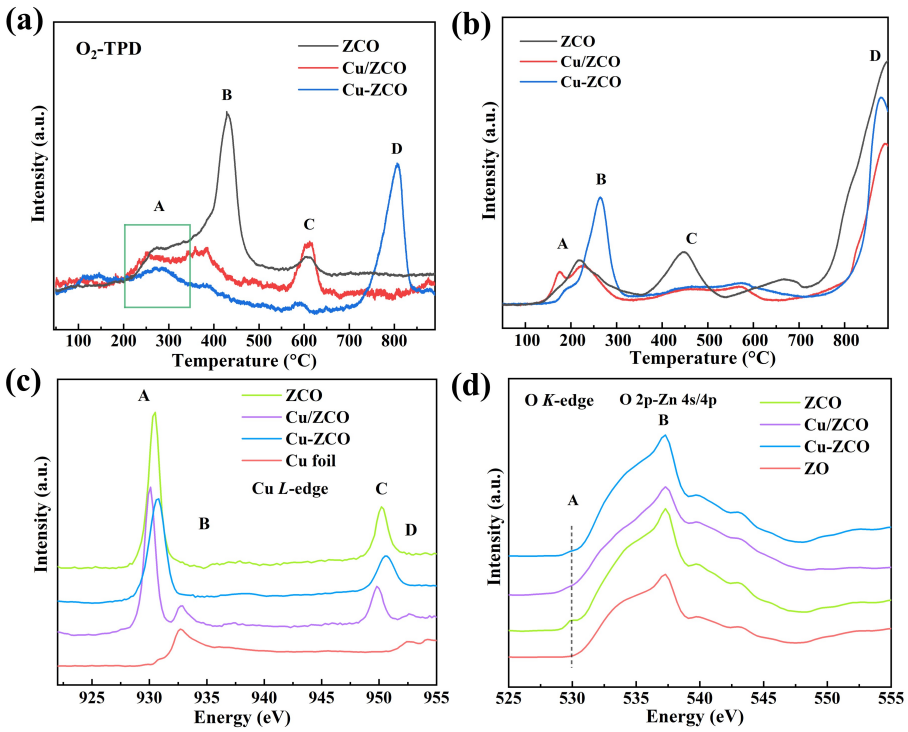


**Figure 5.** (a) $O_2$-temperature-programmed desorption (TPD) profiles and (b) H2-temperatureprogrammed reduction (TPR) profiles of ZCO, Cu/ZCO, and Cu-ZCO; (c) normalized Cu L-edge and (d) normalized O K-edge X-ray absorption near edge structure (XANES) spectra for ZCO, Cu/ZCO, and Cu-ZCO.

To investigate the redox properties of these samples, $O_2$-TPD and $H_2$-TPR profiles were measured. As shown in **Figure 5 a**, it was observed that Cu/ZCO has a strong intensity desorption signal and a lower desorption onset peak temperature than either Cu-ZCO or ZCO, which suggests that Cu/ZCO has a more highly reactive oxygen species. **Figure 5 b** shows that Cu/ZCO has a lower reduction onset peak temperature than either Cu-ZCO or ZCO, and this peak A is considered to represent the reduction of surface adsorbed oxygen species or lattice oxygen. This result is consistent with the data from the online mass spectrometry and $O_2$-TPD, which confirms that the surface lattice oxygen in Cu/ZCO has high reactivity. Heterogeneous catalysis generally occurs at the surface of solid materials, and therefore understanding the relationship between the surface

electronic structure, catalytic activity, and the reaction mechanism can inform about the rational design and development of high-efficiency catalysts. Soft XAS is mainly used to study the surface electronic structure and tends to involve electron transfer and the covalency of metal-oxygen bond, as well as oxidation states.[11, 38] Therefore, the XANES spectrum of the O K-edge and Cu L-edge for ZCO, Cu/ZCO, and Cu-ZCO was recorded. The results for the Cu L-edge XAS are shown in **Figure 5 c and S13a**; XAS spectra of ZnO (ZO) and Cu foil are used as references. On comparing with the Cu L-edge XAS spectrum of ZCO, it is evident that the main absorption peak (peak A and peak C) of the mechanically mixed Cu-ZCO has shifted to lower energy, which indicates that the valence state of the surface Cu has decreased. However, the Cu/ZCO provides different results in the Cu L-edge XAS, where the main peaks A and C shift to lower energy, while the new peak B has a higher energy than the standard Cu foil for this peak position.[39, 40] These results demonstrate that there is a charge transfer between Cu and ZCO in sample Cu/ZCO and that the valence state of the Cu atom in the Cu/ZCO lattice is greater than in ZCO. Meanwhile, Cu-ZCO only displays an average effect for the oxidation state of the Cu, and there is no distinct interaction between the two phases. Furthermore, the normalized oxygen K-edge XAS spectra shown in **Figure 5 d and S13b** reveal that both ZCO and Cu-ZCO have a similar white line peak intensity, which is stronger than that of Cu/ZCO and ZnO. Generally, the white line peak in the X-ray absorption spectrum is considered as the peak with the highest absorption intensity, which is used to study the electron density of the atomic orbit of measured element and the covalence of chemical bonds. Therefore, this result indicates that mechanical mixing has a weak effect on the surface electronic structure of ZCO and that the charge transfer in the Cu/ZCO sample increases the covalency in the Zn-O bond.[38] The disappearance of peak A confirms the transition from CuO to Cu in Cu/ZCO. Therefore, we can infer that the enhanced electron transfer between Cu and ZCO in the Cu/ZCO sample efficiently activates the surface lattice oxygen in the oxide supports.

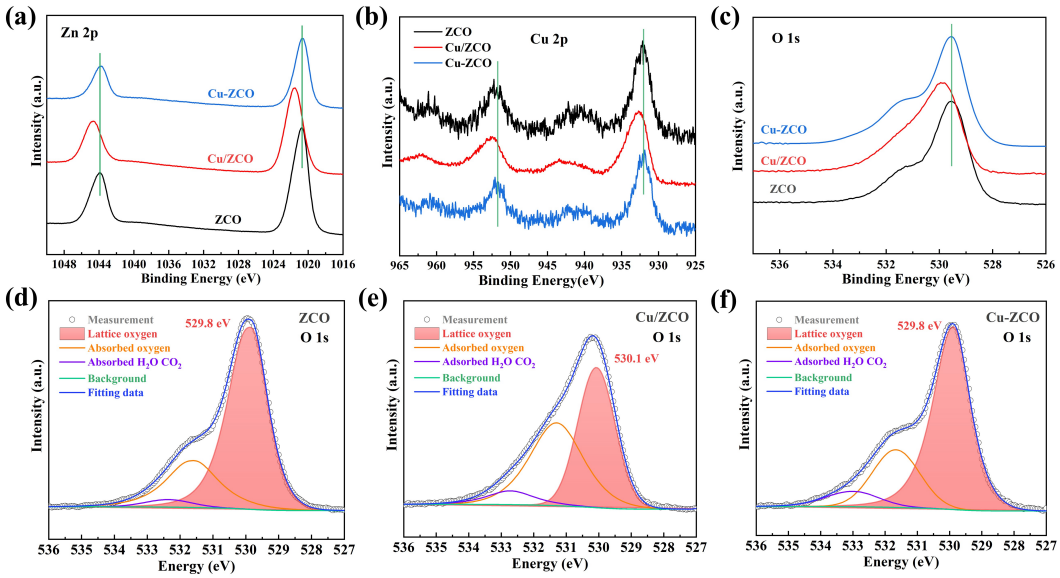


**Figure 6.** (a) Zn 2p, (b) Cu 2p, and (c) O 1s XPS spectrum of ZCO, Cu/ZCO, and Cu-ZCO; detailed fitting peak of (d) ZCO, (e) Cu/ZCO, and (f) Cu-ZCO in the O 1s XPS spectrum.

Surface sensitive tool XPS has been employed to investigate the surface composition and structure of these materials. The Cu 2p, Zn 2p, O 1s, and C 1s XPS spectra are shown in **Figure 6 and S14** and are calibrated using the C 1s XPS spectrum for 284.6 eV (**Figure S7**). It can be observed that the Cu 2p peak in **Figure 6 b** shifts to high energy *versus* Cu-ZCO and ZCO, which indicates that the Cu element in Cu/ZCO possesses a higher oxidation state, while that of Cu-ZCO is the same as that in ZCO. Furthermore, it was found that the Zn 2p XPS spectrum in **Figure 6 a** also shows a similar result to that of the Cu 2p XPS spectrum, where the Zn element in Cu/ZCO possesses a higher oxidation state than that observed for ZCO and Cu-ZCO. These results illustrate that the covalence of the metal-oxygen bond in Cu/ZCO is improved. The O 1s XPS spectrum was measured to analyze the nature and quantity of surface oxygen species present. In **Figure 6 c-f**, the O 1s XPS spectrum is divided into adsorbed oxygen species, adsorbed $CO_2$ species, and surface lattice oxygen. It was found that the peak position of the surface lattice oxygen in Cu/ZCO has undergone an obvious shift to higher binding energy *versus* Cu-ZCO and ZCO (**Figure S15**), and

this indicates that the surface lattice oxygen in Cu/ZCO has higher reactivity.[11, 41] **Figure S16** shows the calculated content of these oxygen species in ZCO, Cu/ZCO, and Cu-ZCO. The ratio of adsorbed oxygen to lattice oxygen in Cu/ZnO (0.94) is larger than that for ZCO (0.4) and Cu-ZCO (0.47). These results demonstrate that the interface interactions in Cu/ZCO change the covalency of the metal-oxygen bond in the support and successfully activate the surface lattice oxygen. In turn, this facilitates the increase of surface adsorbed oxygen species.

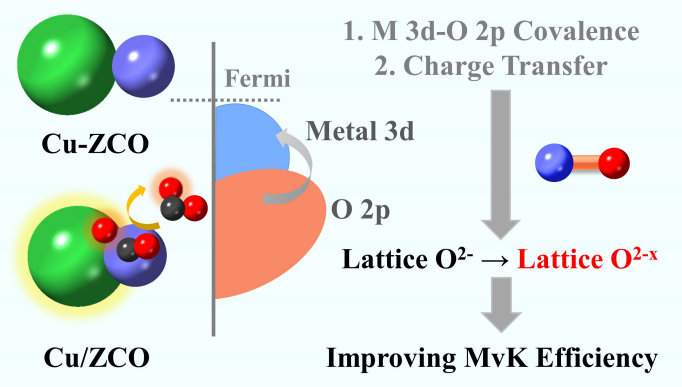


**Figure7.** Schematic illustration of the activation process of the surface lattice oxygen in Cu/ZCO through metal-support interactions (green balls: ZCO, violet balls: Cu nanoparticles, red balls: oxygen atoms, black balls: carbon atoms, and violet blue oxygen balls: Zn/Cu atoms).

Based on the above experimental results of XPS, XAS, on-line MS, and catalytic performance, the relationship between the surface electronic structure, catalytic activity, and reaction mechanism is represented by a schematic illustration. The idea here is to better comprehend the key role played by the surface lattice oxygen. As shown in **Figure 7**, the surface electronic structure of Cu/ZCO obtained by the *in-situ* reduction method is somewhat different from that of Cu-ZCO. Mechanical mixing has a weak effect on the covalency of the metal 3d-O 2p bond in the support, while the covalency of the metal 3d-O 2p bond in Cu/ZCO is prominently improved. Furthermore, Cu/ZCO exhibits an enhanced charge transfer between the Cu and the ZCO support compared to that

observed for Cu-ZCO. These two key elements facilitate the activation of the surface lattice oxygen in Cu-ZCO, namely that the inert lattice oxygen $O^{2-}$ in ZCO is transformed into the active lattice oxygen $O^{2-x}$. This fact has also been confirmed by O 1s XPS (**Figure S15**) and the O K-edge XANES spectrum (**Figure 5 d**). More importantly, $H_2$-TPR and $O_2$-TPD also clarify that surface lattice oxygen in Cu/ZCO is more active than Cu-ZCO and ZCO. This important change dramatically improves the efficiency of the MvK catalytic mechanism in CO oxidation, while the efficiency of the L-H catalytic mechanism remains unchanged. Therefore, Cu/ZCO with active lattice oxygen displays the highest catalytic activity and durability during the CO oxidation process.

## Conclusions

In summary, we have developed a strategy similar to the Trojan horse legend for the *in-situ* preparation of a Cu/ZCO composite catalyst using electrostatic spinning technology. We found that the tailored Cu/ZCO catalyst exhibits strong electron transfer between the Cu metal and the oxide support. The interface interactions can optimize the surface electronic structure of the support, where the covalency of the metal-oxygen bond is enhanced. Based on this, the surface lattice oxygen of Cu/ZCO is efficiently activated and its surface adsorbed oxygen species have also a marked increase. By contrast, the surface electronic structure of a mechanically mixed Cu-ZCO exhibited only weak changes. Furthermore, online isotopic mass spectrometry clarifies that the activation of the surface lattice oxygen in Cu/ZCO dramatically improves the efficiency of the MvK mechanism during the CO oxidation process. In contrast, the reaction efficiency of the L-H mechanism for Cu/ZCO revealed no obvious change *versus* Cu-ZCO. This result demonstrates that the reaction efficiency of the L-H mechanism is mainly related to the surface Cu nanoparticles

on the support, while the MvK mechanism is dominated by the Cu nanoparticle and the activity of the surface lattice oxygen. Therefore, the Cu/ZCO catalyst displays better catalytic activity and durability during the CO oxidation process. Our study provides a novel strategy for the design of composite catalysts and gives insight into the key roles played by the oxide support in catalytic activity, especially the effect of interface interactions on the surface lattice oxygen and reaction process.

## Author Contributions

The manuscript was written through contributions of all authors. All authors have given approval to the final version of the manuscript. M.Z. and X.W. authors contributed equally.

**M.Z.**: experimental operation, some regular characterization studies, scientific drawing, and original draft; **X.W.**: experimental design, data treatment, data analysis, writing-original draft preparation, review, and edition; **Q.Y.**: partial characterization for CO oxidation, $H_2$-TPR and $O_2$-TPD; **X.C.:** XPS and XAS analysis, data discussion, and paper edition/review; **Z.C.**: data discussion and revision; **Z.L.**: in situ FTIR and XAS measurements and data discussion; **C.R.**: language polishing; **C.W.**: TEM and SEM characterizations; **Y.P.**: Online MS measurement and data discussion; **N.W.**: review, edition, supervision, and funding acquisition; **Z.Y., C.R.,** and **W.Y.**: review, edition, revision, and some important guidance.

## Supporting Information

The Supporting Information is available free of charge at this website. Experimental detailed of materials synthesis, detailed characterization techniques, detail CO catalytic oxidation condition; SEM-EDS images, TEM images, 2D histogram of the 10%, 50%, and 90% CO conversion versus reaction temperature, isothermal adsorption curves, pore diameter distribution curves, stability test during the CO oxidation process, in situ DRIFTS of CO adsorption, normalized Cu L-edge XANES spectra, normalized O K-edge XANES spectra, C 1s XPS spectrum, O 1s XPS spectrum, and the ratio of adsorbed oxygen/ lattice oxygen of ZCO, Cu/ZCO, and Cu-ZCO. CO catalytic

oxidation curves of post-annealed Cu-ZCO-A and pre-annealed Cu-ZCO-B, and the element content analysis of ZCO, Cu-ZCO, and Cu/ZCO via ICP and SEM-EDS (PDF).

**Acknowledgments**

This work was supported by the National Natural Science Foundation (51972068), Users with Excellence Program of Hefei Science Center CAS (2020HSC-UE002), and the Natural Science Foundation of Guangxi (2018GXNSFBA138025). Y.A. W acknowledges the Natural Science and Engineering Research Council (NSERC) of Canada (RGPIN-2020–05903 and GECR-2020-00476) for support. CR thanks the EPSRC for an Overseas Travel Grant. The authors thank NSRL beamlines MCD-A and MCD-B (Soochow Beamline for Energy Materials) in National Synchrotron Radiation Laboratory for providing beam time.

**References**

1. Grimaud, A.; Diaz-Morales, O.; Han, B.; Hong, W. T.; Lee, Y.-L.; Giordano, L.; Stoerzinger, K. A.; Koper, M. T. M.; Shao-Horn, Y., Activating Lattice Oxygen Redox Reactions in Metal Oxides to Catalyse Oxygen Evolution. *Nat. Chem.* **2017,** *9*, 457-465.

2. Daelman, N.; Capdevila-Cortada, M.; Lopez, N., Dynamic Charge and Oxidation State of $Pt/CeO_2$ Single-atom Catalysts. *Nat. Mater.* **2019,** *18*, 1215-1221.

3. Nie, L.; Mei, D.; Xiong, H.; Peng, B.; Ren, Z.; Hernandez, X. I. P.; DeLaRiva, A.; Wang, M.; Engelhard, M. H.; Kovarik, L. J. S., Activation of Surface Lattice Oxygen in Single-Atom $Pt/CeO_2$ for Low-temperature CO Oxidation. Science **2017,** *358*, 1419-1423.

4. Assat, G.; Tarascon, J.-M., Fundamental Understanding and Practical Challenges of Anionic Redox Activity in Li-ion Batteries. *Nat. Energy* **2018,** *3*, 373-386.

5. Huang, Z.-F.; Song, J.; Du, Y.; Xi, S.; Dou, S.; Nsanzimana, J. M. V.; Wang, C.; Xu, Z. J.; Wang, X., Chemical and Structural Origin of Lattice Oxygen Oxidation in Co-Zn Oxyhydroxide

Oxygen Evolution Electrocatalysts. *Nat. Energy* **2019,** *4*, 329-338.

6. Hwang, J.; Rao, R. R.; Giordano, L.; Akkiraju, K.; Wang, X. R.; Crumlin, E. J.; Bluhm, H.; Shao-Horn, Y. J. N. C., Regulating Oxygen Activity of Perovskites to Promote $NO_x$ Oxidation and Reduction Kinetics. *Nat. Catal.* **2021**, *4*, 663-673.

7. Zheng, Y.; Thampy, S.; Ashburn, N.; Dillon, S.; Wang, L.; Jangjou, Y.; Tan, K.; Kong, F.; Nie, Y.; Kim, M. J.; Epling, W. S.; Chabal, Y. J.; Hsu, J. W. P.; Cho, K., Stable and Active Oxidation Catalysis by Cooperative Lattice Oxygen Redox on $SmMn_2O_5$ Mullite Surface. *J. Am. Chem. Soc.* **2019,** *141*, 10722-10728.

8. Xiao, Y.; Li, H.; Xie, K. J. A. C. I. E., Activating Lattice Oxygen at the Twisted Surface in a Mesoporous $CeO_2$ Single Crystal for Efficient and Durable Catalytic CO Oxidation. *Angew. Chem. Int. Ed.* **2021,** *60*, 5240-5244.

9. Chen, L.; Chen, P.; Wang, H.; Cui, W.; Sheng, J.; Li, J.; Zhang, Y.; Zhou, Y.; Dong, F., Surface Lattice Oxygen Activation on $Sr_2Sb_2O_7$ Enhances the Photocatalytic Mineralization of Toluene: from Reactant Activation, Intermediate Conversion to Product Desorption. *ACS Appl. Mater. Interfaces* **2021,** *13*, 5153-5164.

10. Hwang, J.; Rao, R. R.; Giordano, L.; Katayama, Y.; Yu, Y.; Shao-Horn, Y. J. S., Perovskites in Catalysis and Electrocatalysis. *Science* **2017,** *358*, 751-756.

11. Wang, X.; Pan, Z.; Chu, X.; Huang, K.; Cong, Y.; Cao, R.; Sarangi, R.; Li, L.; Li, G.; Feng, S., Atomic-Scale Insights into Surface Lattice Oxygen Activation at the Spinel/Perovskite Interface of $Co_3O_4/La_{0.3}Sr_{0.7}CoO_3$. *Angew. Chem. Int. Ed.* **2019,** *58*, 11720-11725.

12. Wang, X.; Huang, K.; Ma, W.; Cong, Y.; Ge, C.; Feng, S., Defect Engineering, Electronic Structure, and Catalytic Properties of Perovskite Oxide $La_{0.5}Sr_{0.5}CoO_{3-\delta}$. *Chem. Eur. J* **2017,** *23*, 1093-1100.

13. Mefford, J. T.; Rong, X.; Abakumov, A. M.; Hardin, W. G.; Dai, S.; Kolpak, A. M.;

Johnston, K. P.; Stevenson, K. J., Water Electrolysis on $La_{1-x}Sr_xCoO_{3-\delta}$ Perovskite Electrocatalysts. *Nat. Commun.* **2016,** *7*, 11053.

14. Wu, Y. A.; McNulty, I.; Liu, C.; Lau, K. C.; Liu, Q.; Paulikas, A. P.; Sun, C.-J.; Cai, Z.; Guest, J. R.; Ren, Y.; Stamenkovic, V.; Curtiss, L. A.; Liu, Y.; Rajh, T., Facet-dependent Active Sites of a Single $Cu_2O$ Particle Photocatalyst for $CO_2$ Reduction to Methanol. *Nat. Energy* **2019,** *4*, 957-968.

15. Polychronopoulou, K.; AlKhoori, A. A.; Efstathiou, A. M.; Jaoude, M. A.; Damaskinos, C. M.; Baker, M. A.; Almutawa, A.; Anjum, D. H.; Vasiliades, M. A.; Belabbes, A.; Vega, L. F.; Zedan, A. F.; Hinder, S. J., Design Aspects of Doped $CeO_2$ for Low-Temperature Catalytic CO Oxidation: Transient Kinetics and DFT Approach. *ACS Appl. Mater. Interfaces* **2021,** *13*, 22391-22415.

16. van Deelen, T. W.; Hernández Mejía, C.; de Jong, K. P., Control of Metal-support Interactions in Heterogeneous Catalysts to Enhance Activity and Selectivity. *Nat. Catal.* **2019,** *2*, 955-970.

17. Wan, J.; Zhao, Z.; Shang, H.; Peng, B.; Chen, W.; Pei, J.; Zheng, L.; Dong, J.; Cao, R.; Sarangi, R.; Jiang, Z.; Zhou, D.; Zhuang, Z.; Zhang, J.; Wang, D.; Li, Y., In Situ Phosphatizing of Triphenylphosphine Encapsulated within Metal-Organic Frameworks to Design Atomic $Co_1–P_1N_3$ Interfacial Structure for Promoting Catalytic Performance. *J. Am. Chem. Soc.* **2020**, *142*, 8431-8439.

18. Shang, H.; Sun, W.; Sui, R.; Pei, J.; Zheng, L.; Dong, J.; Jiang, Z.; Zhou, D.; Zhuang, Z.; Chen, W.; Zhang, J.; Wang, D.; Li, Y., Engineering Isolated $Mn–N_2C_2$ Atomic Interface Sites for Efficient Bifunctional Oxygen Reduction and Evolution Reaction. *Nano Lett.* **2020,** *20*, 5443-5450.

19. Liu, H.; Zakhtser, A.; Naitabdi, A.; Rochet, F.; Bournel, F.; Salzemann, C.; Petit, C.; Gallet, J.-J.; Jie, W., Operando Near-Ambient Pressure X-ray Photoelectron Spectroscopy Study of the CO Oxidation Reaction on the Oxide/Metal Model Catalyst ZnO/Pt(111). *ACS Catal.* **2019,** *9*,

10212-10225.

20. Lee, B.-H.; Park, S.; Kim, M.; Sinha, A. K.; Lee, S. C.; Jung, E.; Chang, W. J.; Lee, K.-S.; Kim, J. H.; Cho, S.-P. J. N. m., Reversible and Cooperative Photoactivation of Single-atom Cu/$TiO_2$ Photocatalysts. *Nat. Mater.* **2019,** *18*, 620-626.

21. Lykaki, M.; Pachatouridou, E.; Carabineiro, S. A. C.; Iliopoulou, E.; Andriopoulou, C.; Kallithrakas-Kontos, N.; Boghosian, S.; Konsolakis, M., Ceria Nanoparticles Shape Effects on the Structural Defects and Surface Chemistry: Implications in CO Oxidation by Cu/$CeO_2$ Catalysts. *Appl. Catal. B: Environ.* **2018,** *230*, 18-28.

22. DeSario, P. A.; Pitman, C. L.; Delia, D. J.; Driscoll, D. M.; Maynes, A. J.; Morris, J. R.; Pennington, A. M.; Brintlinger, T. H.; Rolison, D. R.; Pietron, J. J., Low-temperature CO Oxidation at Persistent Low-valent Cu Nanoparticles on $TiO_2$ Aerogels. *Appl. Catal. B: Environ.* **2019,** *252*, 205-213.

23. Meunier, F. C.; Cardenas, L.; Kaper, H.; Smid, B.; Vorokhta, M.; Grosjean, R.; Aubert, D.; Dembele, K.; Lunkenbein, T., Synergy Between Metallic and Oxidized Pt Sites Unravelled During Room Temperature CO Oxidation on Pt/Ceria. *Angew. Chem. Int. Ed.* **2021,** *60*, 3799-3805.

24. Neagu, D.; Tsekouras, G.; Miller, D. N.; Menard, H.; Irvine, J. T., In Situ Growth of Nanoparticles Through Control of Non-stoichiometry. *Nat. Chem.* **2013,** *5*, 916-923.

25. Neagu, D.; Oh, T. S.; Miller, D. N.; Menard, H.; Bukhari, S. M.; Gamble, S. R.; Gorte, R. J.; Vohs, J. M.; Irvine, J. T., Nano-socketed Nickel Particles with Enhanced Coking Resistance Grown in Situ by Redox Exsolution. *Nat. Commun.* **2015,** *6*, 8120.

26. Hou, N.; Yao, T.; Li, P.; Yao, X.; Gan, T.; Fan, L.; Wang, J.; Zhi, X.; Zhao, Y.; Li, Y., A-Site Ordered Double Perovskite with in Situ Exsolved Core–Shell Nanoparticles as Anode for Solid Oxide Fuel Cells. *ACS Appl. Mater. Interfaces* **2019,** *11*, 6995-7005.

27. Kwon, O.; Sengodan, S.; Kim, K.; Kim, G.; Jeong, H. Y.; Shin, J.; Ju, Y.-W.; Han, J. W.;

Kim, G. J. N. c., Exsolution Trends and Co-segregation Aspects of Self-grown Catalyst Nanoparticles in Perovskites. *Nat. Commun.* **2017,** *8*, 15967.

28. Kuld, S.; Thorhauge, M.; Falsig, H.; Elkjær, C. F.; Helveg, S.; Chorkendorff, I.; Sehested, J. J. S., Quantifying the Promotion of Cu Catalysts by ZnO for Methanol Synthesis. *Science* **2016,** *352*, 969-974.

29. Kattel, S.; Ramírez, P. J.; Chen, J. G.; Rodriguez, J. A.; Liu, P. J. S., Active Sites for $CO_2$ Hydrogenation to Methanol on Cu/ZnO Catalysts. *Science* **2017,** *355*, 1296-1299.

30. Zhang, Z.; Chen, X.; Kang, J.; Yu, Z.; Tian, J.; Gong, Z.; Jia, A.; You, R.; Qian, K.; He, S. J. N. C., The Active Sites of Cu-ZnO Catalysts for Water Gas Shift and CO Hydrogenation Reactions. *Nat. Commun.* **2021,** *12*, 4331.

31. Zhu, H.; Wu, Z.; Su, D.; Veith, G. M.; Lu, H.; Zhang, P.; Chai, S. H.; Dai, S., Constructing Hierarchical Interfaces: $TiO_2$-Supported PtFe-$FeO_x$ Nanowires for Room Temperature CO Oxidation. *J. Am. Chem. Soc.* **2015,** *137*, 10156-10159.

32. Davó-Quiñonero, A.; Bailón-García, E.; López-Rodríguez, S.; Juan-Juan, J.; Lozano-Castelló, D.; García-Melchor, M.; Herrera, F. C.; Pellegrin, E.; Escudero, C.; Bueno-López, A., Insights into the Oxygen Vacancy Filling Mechanism in $CuO/CeO_2$ Catalysts: A Key Step Toward High Selectivity in Preferential CO Oxidation. *ACS Catal.* **2020,** *10*, 6532-6545.

33. Roy, C.; Sebok, B.; Scott, S. B.; Fiordaliso, E. M.; Sørensen, J. E.; Bodin, A.; Trimarco, D. B.; Damsgaard, C. D.; Vesborg, P. C. K.; Hansen, O.; Stephens, I. E. L.; Kibsgaard, J.; Chorkendorff, I., Impact of Nanoparticle Size and Lattice Oxygen on Water Oxidation on $NiFeO_xH_y$. *Nat. Catal.* **2018**, *1*, 820-829.

34. Kothari, M.; Jeon, Y.; Miller, D. N.; Pascui, A. E.; Kilmartin, J.; Wails, D.; Ramos, S.; Chadwick, A.; Irvine, J. T. J. N. C., Platinum Incorporation into Titanate Perovskites to Deliver Emergent Active and Stable Platinum Nanoparticles. *Nat. Chem.* **2021**, *13*, 677-682.

35. Zheng, B.; Gan, T.; Shi, S.; Wang, J.; Zhang, W.; Zhou, X.; Zou, Y.; Yan, W.; Liu, G., Exsolution of Iron Oxide on $LaFeO_3$ Perovskite: A Robust Heterostructured Support for Constructing Self-Adjustable Pt-Based Room-Temperature CO Oxidation Catalysts. *ACS Appl. Mater. interfaces* **2021**, *13*, 27029-27040.

36. Gan, T.; Yang, J.; Morris, D.; Chu, X.; Zhang, P.; Zhang, W.; Zou, Y.; Yan, W.; Wei, S.-H.; Liu, G., Electron Donation of Non-oxide Supports Boosts $O_2$ Activation on Nano-platinum Catalysts. *Nat. Commun.* **2021,** *12*, 2741.

37. Noei, H.; Birkner, A.; Merz, K.; Muhler, M.; Wang, Y., Probing the Mechanism of Low-Temperature CO Oxidation on Au/ZnO Catalysts by Vibrational Spectroscopy. *J. Phys. Chem. C* **2012,** *116*, 11181-11188.

38. Wang, X.; Huang, K.; Yuan, L.; Xi, S.; Yan, W.; Geng, Z.; Cong, Y.; Sun, Y.; Tan, H.; Wu, X.; Li, L.; Feng, S., Activation of Surface Oxygen Sites in a Cobalt-Based Perovskite Model Catalyst for CO Oxidation. *J. Phys. Chem. Lett.* **2018,** *9*, 4146-4154.

39. Chou, T. C.; Chang, C. C.; Yu, H. L.; Yu, W. Y.; Dong, C. L.; Velasco-Velez, J. J.; Chuang, C. H.; Chen, L. C.; Lee, J. F.; Chen, J. M.; Wu, H. L., Controlling the Oxidation State of the Cu Electrode and Reaction Intermediates for Electrochemical $CO_2$ Reduction to Ethylene. *J. Am. Chem. Soc.* **2020**, *142*, 2857-2867.

40. Liu, H.; Guo, J.; Yin, Y.; Augustsson, A.; Dong, C.; Nordgren, J.; Chang, C.; Alivisatos, P.; Thornton, G.; Ogletree, D. F. J. N. L., Electronic Structure of Cobalt Nanocrystals Suspended in Liquid. *Nano Lett.* **2007,** *7*, 1919-1922.

41. Wang, X.; Li, X.; Chu, X.; Cao, R.; Qian, J.; Cong, Y.; Huang, K.; Wang, J.; Redshaw, C.; Sarangi, R.; Li, G.; Feng, S., Manipulating Surface Termination of Perovskite Manganate for Oxygen Activation. *Adv. Funct. Mater.* **2021,** *31*, 2006439.